Tracing Streamlines on Unstructured Grids From Finite Volume Discretizations

S.F. Matringe, SPE, Stanford University, **R. Juanes,** SPE, Massachusetts Institute of Technology, **H.A. Tchelepi,** SPE, Stanford University.

Summary

The accuracy of streamline reservoir simulations depends strongly on the quality of the velocity field and the accuracy of the streamline tracing method. For problems described on complex grids (e.g., corner-point geometry or fully unstructured grids) with full-tensor permeabilities, advanced discretization methods, such as the family of multipoint flux approximation (MPFA) schemes, are necessary to obtain an accurate representation of the fluxes across control volume faces. These fluxes are then interpolated to define the velocity field within each control volume, which is then used to trace the streamlines. Existing methods for the interpolation of the velocity field and integration of the streamlines do not preserve the accuracy of the fluxes computed by MPFA discretizations.

Here we propose a method for the reconstruction of the velocity field with high-order accuracy from the fluxes provided by MPFA discretization schemes. This reconstruction relies on a correspondence between the MPFA fluxes and the degrees of freedom of a mixed finite-element method (MFEM) based on the first-order Brezzi-Douglas-Marini space. This link between the finite-volume and finite-element methods allows the use of flux reconstruction and streamline tracing techniques developed previously by the authors for mixed finite elements. After a detailed description of our streamline tracing method, we study its accuracy and efficiency using challenging test cases.

Introduction

The next-generation reservoir simulators will be unstructured. Several research groups throughout the industry are now developing a new breed of reservoir simulators to replace the current industry standards. One of the main advances offered by these next-generation simulators is their ability to support unstructured or, at least, strongly distorted grids populated with full-tensor permeabilities.

The constant evolution of reservoir modeling techniques provides an increasingly realistic description of the geological features of petroleum reservoirs. To discretize the complex geometries of geocellular models, unstructured grids seem to be a natural choice. Their inherent flexibility permits the precise description of faults, flow barriers, trapping structures, etc. Obtaining a similar accuracy with more traditional structured grids, if at all possible, would require an overwhelming number of gridblocks.

However, the added flexibility of unstructured grids comes with a cost. To accurately resolve the full-tensor permeabilities or the grid distortion, a two-point flux approximation (TPFA) approach, such as that of classical finite difference (FD) methods is not sufficient. The size of the discretization stencil needs to be increased to include more pressure points in the computation of the fluxes through control volume edges. To this end, multipoint flux approximation (MPFA) methods have been developed and applied quite successfully (Aavatsmark et al. 1996; Verma and Aziz 1997; Edwards and Rogers 1998; Aavatsmark et al. 1998b; Aavatsmark et al. 1998c; Aavatsmark et al. 1998a; Edwards 2002; Lee et al. 2002a; Lee et al. 2002b).

In this paper, we interpret finite volume discretizations as MFEM for which streamline tracing methods have already been developed (Matringe et al. 2006; Matringe et al. 2007b; Juanes and Matringe In Press). This approach provides a natural way of reconstructing velocity fields from TPFA or MPFA fluxes. For finite difference or TPFA discretizations, the proposed interpretation provides mathematical justification for Pollock's method (Pollock 1988) and some of its extensions to distorted grids (Cordes and Kinzelbach 1992; Prévost et al. 2002; Hægland et al. 2007; Jimenez et al. 2007). For MPFA, our approach provides a high-order streamline tracing algorithm that takes full advantage of the flux information from the MPFA discretization.

Streamline Simulation

Streamline simulation is a fast alternative to classical reservoir simulation methods. To illustrate the difference between traditional and streamline-based simulations, we take the example of an immiscible two-phase displacement process, with negligible capillarity and gravity forces. A more complete introduction to streamline methods can be found in Batycky et al. (1997), Bratvedt et al. (1993) or King and Datta-Gupta (1998).

The flow problem, which describes the evolution of the pressure p, is formed by the combination of Darcy's law

$$u = -\lambda k \nabla p, \qquad (1)$$

and a mass balance condition

$$\nabla \cdot u = g. \qquad (2)$$

In Eqs. 1 and 2, u is the total Darcy velocity, λ the total fluid mobility, k a full permeability tensor, and g a source term. The combination of Eqs. 1 and 2 yields the classical elliptic flow problem

$$\nabla \cdot (-\lambda k \nabla p) = g. \qquad (3)$$

The transport problem, which describes the evolution of the saturation S, follows a hyperbolic mass conservation equation:

$$\phi \frac{\partial S}{\partial t} + u \cdot \nabla f = 0, \qquad (4)$$

where ϕ is the porosity of the medium and f is the fractional flow function.

In traditional reservoir simulation, Eqs. 3 and 4 are solved simultaneously through a finite volume approach (Aziz and Settari 1979). In streamline simulation, the time-of-flight variable τ is introduced to recast the transport problem into a series of independent 1D equations along streamlines (Datta-Gupta and King 1995):

$$\frac{\partial S}{\partial t} + \frac{\partial f}{\partial \tau} = 0. \qquad (5)$$

Physically, τ describes the travel time of a fluid particle along a streamline. The performance of streamline simulation emanates from this modified formulation of the transport problem, which, instead of being solved globally, can now be solved as a series of simpler one-dimensional problems.

Streamline methods use a sequential approach to solve the flow and the modified transport problem. First, the flow problem is solved on the simulation grid to obtain the pressure solution at a given time and the streamlines are traced. Second, the modified transport problem is posed along the streamlines where the saturations are advected following Eq. 5. The quality of the streamlines in terms of location and time-of-flight is therefore crucial to the accuracy of the overall simulation.

This paper (SPE 103295) was accepted for presentation at the 2006 SPE Annual Technical Conference and Exhibition, San Antonio, Texas, U.S.A., 24-27 September 2006, and revised for publication. Original manuscript received for review 10 July 2006. Revised manuscript received for review 17 January 2008. Paper peer approved 8 February 2008.

A streamline tracing method is usually based on a fluid particle-tracking concept. First the velocity field is reconstructed from the pressure solution to the flow problem. This velocity field is then integrated by following the path of a fluid particle in time. This integration is usually performed to arbitrary precision, either analytically or numerically depending on the complexity of the velocity field. Therefore, the real challenge in tracing accurate streamlines is to reconstruct an accurate velocity field. This reconstruction depends on the discretization used for the pressure equation. The next two sections present how to perform this reconstruction for MFEM and finite volume methods on general triangular or quadrilateral grids.

Streamline Tracing Based on MFEM

The Mixed Finite Element Method. Assuming, for simplicity, that the relative mobility λ is constant (unit-mobility ratio displacements), Eqs. 1 and 2 can be expressed as:

$$\mathbf{k}^{-1}u+\nabla p=0, \quad (6)$$

$$\nabla\cdot u=g. \quad (7)$$

The essence of the mixed finite element method is to solve for pressure p and velocity u simultaneously. As in any other finite element procedure, the pressure and velocity fields are interpolated from the pressure and flux unknowns using shape functions with local support:

$$u\approx\sum_{i=1}^{n_{\text{edge}}}U_iN_i^u, \quad (8)$$

$$p\approx\sum_{j=1}^{n_{\text{elem}}}P_jN_j^p, \quad (9)$$

where N_i^u and N_j^p are the velocity and pressure shape functions, respectively, and U_i and P_j are the corresponding flux and pressure unknowns defined on the simulation grid, respectively.

The pressure and velocity spaces cannot be chosen independently of each other. To obtain a convergent approximation, they must satisfy two conditions (Brezzi and Fortin 1991; Brenner and Scott 1994): a standard coercivity condition, and the discrete inf–sup condition (Babuška 1973; Brezzi 1974). Here, we restrict our attention to spaces that satisfy the inf–sup condition in combination with a discretization of the pressure field that is constant over each element. Two well-known spaces are compatible with the chosen pressure discretization: the lowest-order Raviart–Thomas space, RT_0, (Raviart and Thomas 1977) and the Brezzi–Douglas–Marini space of order one, BDM_1, (Brezzi et al. 1985). These are discussed below.

Low-Order Velocity Field. Velocity fields in RT_0 are described by a constant normal trace along element edges, as sketched in **Fig. 1.** Knowledge of the fluxes across each of the edges of an element is sufficient to fully describe the RT_0 velocity field. Thus, only one velocity degree of freedom per edge is needed and, therefore, three degrees of freedom are needed to fully characterize RT_0 on triangles and four on quadrilaterals **(Fig. 2).**

High-Order Velocity Field. This space improves the description of the velocity field by allowing a linear variation of the normal trace of the velocity along element edges, as depicted in **Fig. 3.** One extra degree of freedom per edge is available for the description of the velocity, which brings the dimensionality of BDM_1 to 6 for triangular elements, and 8 for quadrilaterals.

Treatment of Grid Distortion. The proposed streamline tracing algorithm is defined in a reference space. This allows for a more robust and efficient implementation of the algorithm. Thus, we define a mapping φ that describes the relationship between the reference

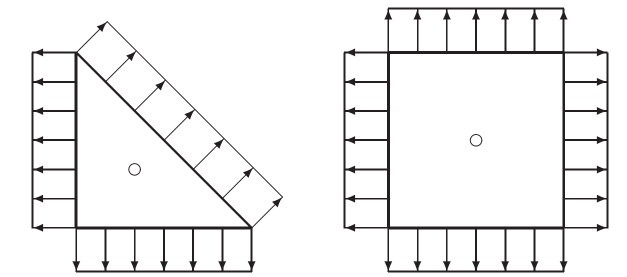

Fig. 1—RT_0 velocity fields are described by a constant velocity profile on element edges.

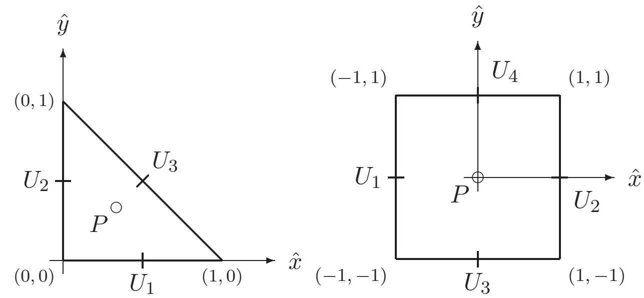

Fig. 2—Location of the pressure (P) and flux (U_1–U_4) unknowns on the reference triangular and quadrilateral elements for the lowest-order RT_0 discretization.

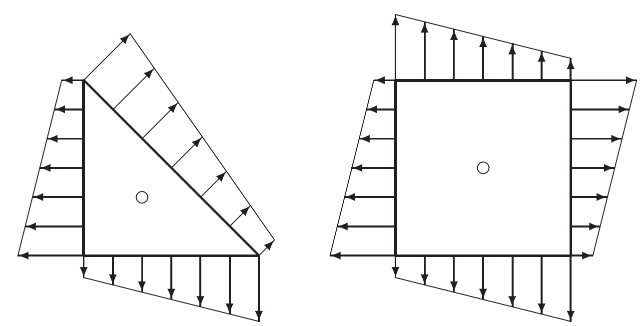

Fig. 3—BDM_1 velocity fields are described by a linearly varying normal trace along element edges.

coordinates $\hat{x}$ in the reference element $\hat{K}$ and the physical coordinates x in the distorted element K **(Figs. 4 and 5).**

$$\varphi:\begin{cases}\mathbb{R}^2 & \to\mathbb{R}^2\\ \hat{x}\in\hat{K} & \mapsto x=\varphi(\hat{x})\in K\end{cases} \quad (10)$$

For all gridcells, the mapping φ must be invertible and sufficiently smooth. This guarantees that the Jacobian matrix of the transformation $D(\hat{x})=\partial\varphi/\partial\hat{x}$ is invertible and that its determinant $J(\hat{x})=\det D(\hat{x})$ is non zero. The mapping φ is taken as the classical isoparametric mapping, which is defined as an interpolation of the nodal coordinates x_a in physical space:

$$x=\varphi(\hat{x})=\sum_{a=1}^{n_{\text{node}}}N_a(\hat{x})x_a, \quad (11)$$

where N_a are the classical finite element shape functions:

$$N_1(\hat{x})=1-\hat{x}-\hat{y},\quad N_2(\hat{x})=\hat{x},\ \text{and}\ N_3(\hat{x})=\hat{y} \quad (12)$$

for triangular elements, and

$$N_1=\frac{(1-\hat{x})(1-\hat{y})}{4},\quad N_2=\frac{(1+\hat{x})(1-\hat{y})}{4},$$
$$N_3=\frac{(1+\hat{x})(1+\hat{y})}{4},\quad N_4=\frac{(1-\hat{x})(1+\hat{y})}{4}, \quad (13)$$

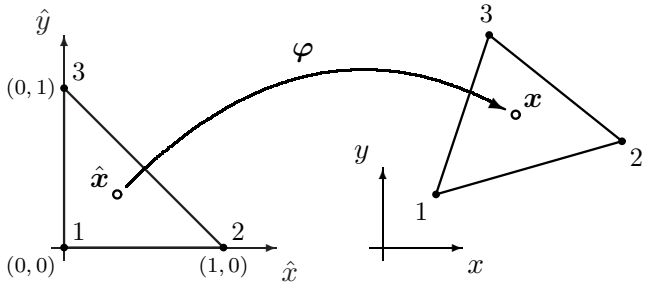

Fig. 4—Mapping for triangular elements.

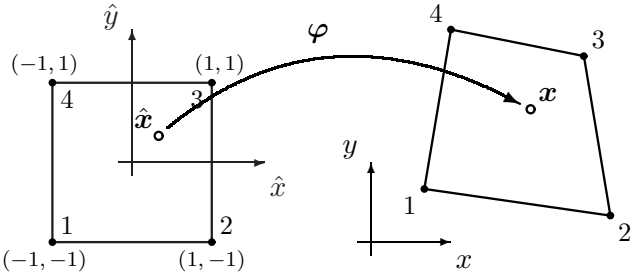

Fig. 5—Mapping for quadrilateral elements.

for quadrilateral elements.

In addition to the coordinate mapping, working in a reference element requires to map vector fields. The classical Piola transform (Brezzi and Fortin 1991; Marsden and Hughes 1994) is used to map the velocity field:

$$v(x) = \mathcal{P}(\hat{v})(x) = \frac{1}{J(\hat{x})} D(\hat{x})\hat{v}(\hat{x}), \quad \ldots\ldots\ldots\ldots\ldots\ldots \quad (14)$$

with v and $\hat{v}$ the velocity fields in the physical and reference spaces, respectively. The essential property of the Piola transform is that it preserves the normal trace of vector fields, which, in our case, translates into the conservation of the fluxes through control volume faces between the reference and physical spaces.

The introduction of the isoparametric mapping for the coordinates and the Piola transform for the velocity field reduces the problem of streamline tracing on deformed elements to that of tracing on reference elements (Cordes and Kinzelbach 1992; Prévost et al. 2002).

Integration of the Streamline Path. Once the velocity field is reconstructed within an element, it can be integrated to yield the streamline path. Juanes and Matringe (In Press) showed that both the Raviart-Thomas and Brezzi-Douglas-Marini families of vector fields yield a stream function and provided the form of these functions. For these velocity fields, the streamline path is therefore known analytically (Matringe et al. 2006; Matringe et al. 2007b).

However, both the streamline path and time-of-flight are needed to solve the transport problem in streamline simulation. The time-of-flight is defined as the travel time of a fluid particle along a streamline (Datta-Gupta and King 1995):

$$\tau = \int_{\mathcal{L}} \frac{1}{|u(s)|}\, \mathrm{d}s, \quad \ldots\ldots\ldots\ldots\ldots\ldots\ldots\ldots \quad (15)$$

where s represents the arc length along the streamline $\mathcal{L}$. The Piola transform and isoparametric mapping are used to express Eq. 15 in the reference space:

$$\tau = \int_{\hat{\mathcal{L}}} \frac{1}{|\hat{u}(\hat{s})|} J(\hat{x})\, \mathrm{d}\hat{s}. \quad \ldots\ldots\ldots\ldots\ldots\ldots\ldots \quad (16)$$

In general, the integrand of Eq. 16 is too complex for an analytical integration and must be integrated numerically. There are two notable exceptions: (1) in triangular elements, because the isoparametric mapping is affine and the Jacobian $J(\hat{x})$ is therefore constant; (2) in rectangular elements where the mapping φ is also affine and Pollock's method (Pollock 1988) can then be used for an analytical integration of the time-of-flight. In the numerical examples presented in this paper, the time-of-flight is always integrated numerically using an explicit Runge-Kutta (4,5) integration to machine precision (Dormand and Prince 1980).

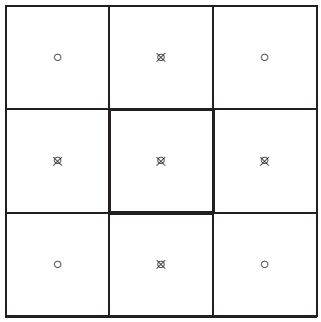

Fig. 6—Five-point (×) and nine-point (○) stencils corresponding to the TPFA and MPFA methods, respectively.

Streamline Tracing Based on MPFA

The MPFA Method. In reservoir simulation, finite volume (FV) methods are typically used for the discretization of Eq. 3. The simulation grid is formed by N nonoverlapping cells K_j that span completely the simulation domain Ω:

$$\Omega = \bigoplus_{j=1}^{N} K_j. \quad \ldots\ldots\ldots\ldots\ldots\ldots\ldots\ldots\ldots\ldots \quad (17)$$

In this paper, we consider partitions of Ω formed by general triangular and quadrilateral cells. Each gridcell K_j is used as a control volume to enforce an integral form of the mass balance condition of Eq. 2:

$$\int_{K_j} \nabla \cdot u \, \mathrm{d}\Omega = \int_{K_j} g \, \mathrm{d}\Omega. \quad \ldots\ldots\ldots\ldots\ldots\ldots\ldots \quad (18)$$

Let Γ_j be the boundary of K_j and n the outward unit vector normal to Γ_j. Using the divergence theorem, we rewrite the mass balance condition on the control volume as:

$$F = \int_{\Gamma_j} u \cdot n \, \mathrm{d}\Gamma = \int_{K_j} g \, \mathrm{d}\Omega, \quad \ldots\ldots\ldots\ldots\ldots\ldots \quad (19)$$

where F is defined as the flux out of the control volume K_j. FV methods approximate F as a sum over the cell edges by interpolation from neighboring pressure nodes. The number of pressure nodes used to compute a given flux defines the stencil of the FV method. A larger stencil increases the number of connections between cells. This usually leads to a more accurate but more costly solution. The two main types of FV methods used in reservoir simulation are TPFA and MPFA.

In TPFA, the flux across an interface is computed using the pressure nodes located at the center of the two gridblocks sharing their boundary. This leads to the classic five-point stencil on structured quadrilateral grids **(Fig. 6).** TPFA cannot, however, account properly for grid distortion or full-tensor permeabilities.

MPFA methods were developed to discretize the flow problem on advanced grids. An excellent introduction (including an extensive literature review) to MPFA discretization is given by Aavatsmark (2002). To take into account more accurately the grid distortion or full-tensor permeabilities, the MPFA stencil is extended. The flux through the i^{th} interface is now interpolated as

$$F_i = \sum_{j \in J} T_{ij} p_j, \quad \ldots\ldots\ldots\ldots\ldots\ldots\ldots\ldots \quad (20)$$

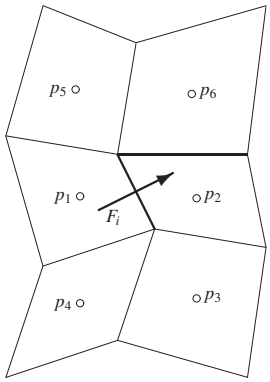

Fig. 7—MPFA stencil.

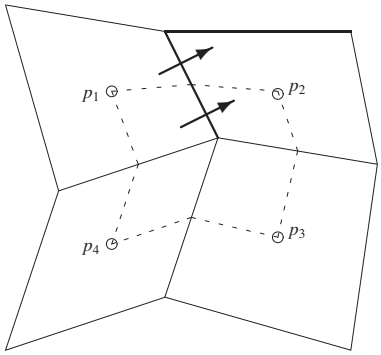

Fig. 8—Interaction region (dashed line) for a subinterface flux in MPFA.

where T_{ij} is a transmissibility coefficient and J the set of gridblocks that share a node with the i^{th} interface. For a structured quadrilateral grid, six pressure nodes are therefore used to compute a flux **(Fig. 7),** which leads to a nine-point stencil (Fig. 6).

To compute the transmissibility coefficients T_{ij} of Eq. 20, a dual grid is created. This dual grid is staggered with respect to the primal grid defining the gridblocks. Each cell of the dual grid is referred to as an interaction region and is centered on a node of the primal grid **Fig. 8).**

The interaction regions divide each cell interface into two subinterfaces. The transmissibility coefficients of Eq. 20 are obtained by solving local problems on the interaction regions. This local problem is defined through an approach similar to that of the 1D problem. The pressure is assumed to vary linearly within each gridblock and is constrained by pressure and flux continuity conditions across subinterfaces. Because it is usually impossible to obtain full pressure and flux continuity across subinterfaces, the pressure continuity constraints are only weakly enforced. The existing MPFA methods differ mainly in the way this weak pressure continuity is enforced.

The important point is that MPFA computes two subfluxes per edge. These subfluxes correspond to the flux of the velocity field through each half-edge. The total flux through the edge is the sum of these two subfluxes. For an MPFA discretization, the reconstruction of the velocity field can be based either on the total fluxes or on the subfluxes.

Our strategy to reconstruct the MPFA velocity fields is to interpret the total fluxes or subfluxes provided by MPFA as MFEM degrees of freedom. The shape functions of the MFEM velocity spaces are then used to interpolate the MPFA fluxes and yield a continuous velocity field within the control volume that is consistent with the discrete fluxes provided by the MPFA discretization. The velocity fields so defined are guaranteed to be divergence-free, curl-free and to yield a stream function (Juanes and Matringe In Press).

Low-Order Tracing—Pollock's Method. The RT_0 space is used to reconstruct velocity fields defined by the total MPFA fluxes. Since the RT_0 degrees of freedom are defined as the total fluxes through element edges, we write the reconstructed velocity in the reference space as

$$\hat{v}(\hat{x}) = \sum_{e=1}^{n_e} F_e N_e(\hat{x}), \quad \ldots\ldots\ldots\ldots\ldots\ldots\ldots \quad (21)$$

with n_e the number of edges per element, F_e the total MPFA flux through edge e and N_e the RT_0 shape function corresponding to edge e. For the reference triangle, $n_e = 3$ and

$$N_1 = (\hat{x}, -1+\hat{y})^t, \quad N_2 = (\hat{x}, \hat{y})^t, \text{ and}$$
$$N_3 = (-1+\hat{x}, \hat{y})^t. \quad \ldots\ldots\ldots \quad (22)$$

For the reference square, $n_e = 4$ and

$$N_1 = \frac{1}{4}(0, -1+\hat{y})^t, \quad N_2 = \tfrac{1}{4}(\ 1+\hat{x}, 0)^t,$$
$$N_3 = \frac{1}{4}(0,\ 1+\hat{y})^t, \quad N_4 = \tfrac{1}{4}(-1+\hat{x}, 0)^t. \quad \ldots\ldots \quad (23)$$

On Cartesian grids, we recover Pollock's method (Pollock 1988). On general quadrilateral grids, with the coordinate mapping of Eq. 11 and the Piola transform of Eq. 14, we obtain the extension of Pollock's method to distorted grids proposed by Cordes and Kinzelbach (1992).

High-Order Tracing. To reconstruct a higher-order velocity field, the two subfluxes provided by MPFA on each edge are used. The BDM_1 space defines the interpolated velocity field in the reference space as

$$\hat{v}(\hat{x}) = \sum_{e=1}^{n_e} \sum_{i=1}^{2} f_{e,i} N_{e,i}(\hat{x}), \quad \ldots\ldots\ldots\ldots\ldots\ldots\ldots \quad (24)$$

where $f_{e,i}$ $(i = 1,2)$ are the MPFA subfluxes associated with edge e. $N_{e,i}$ are the BDM_1 shape functions on the reference triangle:

$$N_{1,1} = (0,\ -1+\hat{x}+\hat{y})^t, \quad N_{1,2} = (\hat{x},\ -\hat{x})^t,$$
$$N_{2,1} = (\hat{x},\ 0)^t, \quad N_{2,2} = (0,\ \hat{y})^t,$$
$$N_{3,1} = (-1+\hat{x}+\hat{y},\ 0)^t, \quad N_{3,2} = (-\hat{y},\ \hat{y})^t. \quad \ldots\ldots \quad (25)$$

or on the reference quadrilateral:

$$N_{1,1} = \tfrac{1}{4}\left(-(1-\hat{x}^2)/2, \quad (1-\hat{x})(-1+\hat{y})\right)^t,$$
$$N_{1,2} = \tfrac{1}{4}\left(\ (1-\hat{x}^2)/2, \quad (1+\hat{x})(-1+\hat{y})\right)^t,$$
$$N_{2,1} = \tfrac{1}{4}\left((1+\hat{x})(1-\hat{y}), \quad -(1-\hat{y}^2)/2\right)^t,$$
$$N_{2,2} = \tfrac{1}{4}\left((1+\hat{x})(1+\hat{y}), \quad (1-\hat{y}^2)/2\right)^t,$$
$$N_{3,1} = \tfrac{1}{4}\left(\ (1-\hat{x}^2)/2, \quad (1+\hat{x})(1+\hat{y})\right)^t,$$
$$N_{3,2} = \tfrac{1}{4}\left(-(1-\hat{x}^2)/2, \quad (1-\hat{x})(1+\hat{y})\right)^t,$$
$$N_{4,1} = \tfrac{1}{4}\left((-1+\hat{x})(1+\hat{y}), \quad (1-\hat{y}^2)/2\right)^t,$$
$$N_{4,2} = \tfrac{1}{4}\left((-1+\hat{x})(1-\hat{y}), \quad -(1-\hat{y}^2)/2\right)^t, \quad \ldots \quad (26)$$

The idea of using the MPFA subfluxes in the velocity reconstruction was first introduced by Prévost et al. (2002). To trace streamlines, Prévost et al. proposed to divide each control volume into subcells, defined as the regions of the control volume delimited by the MPFA interaction regions. A flux post-processing technique was used to recover fluxes through the edges of the interaction regions. The

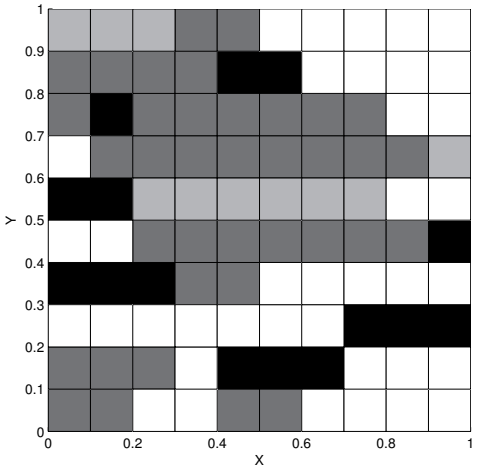

Fig. 9—Heterogeneous permeability field from Mosé et al. (1994). Permeability values: white$= 1$; light gray$= 10^{-1}$; dark gray$= 10^{-2}$; black$= 10^{-3}$.

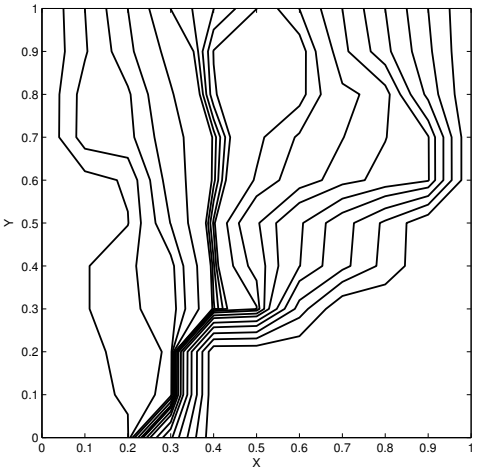

Fig. 10—MPFA streamlines from the RT_0 and BDM_1–based tracing (overlapping exactly).

streamlines were then traced on each subcell using the extension of Pollock's algorithm to distorted grids.

Using BDM_1 to trace streamlines offers two advantages over the approach of Prévost et al. First, BDM_1 provides a velocity field with linearly varying normal components over control-volume edges, which is more accurate than the piecewise constant approximation obtained by Prévost et al. Second, the BDM_1-based tracing does not require a flux recovery procedure since the velocity field is directly interpolated from the subfluxes provided by the MPFA discretization.

Numerical Results

In this section, we compare the streamlines obtained with the low-order and high-order tracing methods described previously, obtained from the same MPFA solution of the pressure equation. The differences are caused exclusively by the amount of information used for the velocity reconstruction: only the MPFA edge fluxes in the low-order RT_0-based tracing, and the MPFA half-edge fluxes in the high-order BDM_1-based tracing. Moreover, because they emanate from the same pressure solution and because their path is known analytically, no significant or consistent difference was observed in the computational cost of both sets of streamlines. The differences in computational cost are solely because of the numerical integration of the time-of-flight, which was not found to depend strongly on the type of velocity field used.

Permeability Heterogeneity. Reservoir heterogeneity is a key component of any reservoir model. It is therefore crucial for a streamline tracing algorithm to accurately handle the discontinuities of permeability fields.

To isolate the influence of the permeability heterogeneity from that of permeability anisotropy or grid distortion, we simulate a problem on a Cartesian grid populated with heterogeneous but isotropic permeability. We used a test case proposed by Mosé et al. (1994), designed to compare the performance of various discretization methods in the presence of heterogeneity. The permeability field used in this test case is shown in **Fig. 9.** Four orders of magnitudes of permeability variations represent flow barriers and high-permeability streaks that force the streamlines to meander through the domain. A unit pressure is set at the top boundary and a zero pressure at the bottom. The left and right domain boundaries are impermeable. Streamlines are launched at equidistant points located at the top of the domain.

On a Cartesian grid and with a diagonal permeability tensor, MPFA reduces to the classical 5-point stencil of TPFA. Because the diagonal points are not included in the stencil, both subedge transmissibilities associated with a given interface are equal, which leads to a constant velocity profile through any given edge. For validation purposes, we here check that both the low- and high-order tracing algorithms recover identical streamlines. The streamlines obtained from both methods are plotted in **Fig. 10.** A single set of streamlines is visible as they overlap exactly. As expected, both tracing methods result in identical time-of-flights as well.

Grid Distortion and Full-Tensor Permeability. A full permeability tensor is required for the description of anisotropic permeability fields with principal directions misaligned with the simulation grid.

In this example, we test the ability of our streamline tracing algorithm to enhance the velocity description and streamline quality in the presence of full tensor permeabilities. The first test case is based on a strongly distorted quadrilateral grid shown in **Fig. 11** and formed by chevron-shaped elements exhibiting a 70° distortion angle. To test the tracing methods on a triangular grid, each quadrilateral of the chevron grid was also split in two triangles to form the grid shown in **Fig. 12.**

The domain has impermeable boundaries, and pressure boundary conditions are set following a quarter of a five spot pattern: Unit pressure is fixed at the bottom-left gridblock, and zero pressure is imposed at the top-right cell.

The permeability field is homogeneous but presents a 10:1 anisotropy ratio and is rotated by a 45° angle from the principal coordinate system:

$$k = R^t \begin{pmatrix} 10 & 0 \\ 0 & 1 \end{pmatrix} R = \begin{pmatrix} 5.5 & 4.5 \\ 4.5 & 5.5 \end{pmatrix}, \quad \ldots\ldots\ldots\ldots \quad (27)$$

with the rotation matrix R defined by

$$R = \begin{pmatrix} \cos(45^\circ) & \sin(45^\circ) \\ -\sin(45^\circ) & \cos(45^\circ) \end{pmatrix}. \quad \ldots\ldots\ldots\ldots\ldots \quad (28)$$

The MPFA method leads to a nine-point stencil on the quadrilateral grid and, in this case, the contributions of the diagonal entries of the stencil are expected to be significant. To compare the streamlines traced with the classical and higer-order flux reconstruction techniques, we used a reference solution defined with the same boundary conditions and permeability field, but computed on a 100×100 Cartesian grid and solved with a BDM_1 MFEM.

Figs. 11 and 12 present the pressure solutions and reference streamlines, and compare the low-order and high-order streamlines obtained on the quadrilateral and triangular grids, respectively. **Table 1** reports the relative error in time-of-flight recorded for each streamline, with respect to the reference streamlines obtained on the refined grid with the mixed finite element method. The streamlines are numbered from the top to the bottom. The average time of flight error is also presented.

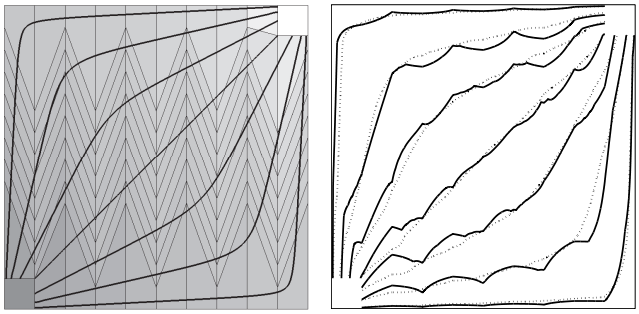

Fig. 11—Left: pressure solution on the quadrilateral chevron grid and reference streamlines. Right: streamlines traced on the quadrilateral chevron grid with the RT_0 (solid lines) and BDM_1 (dotted lines) velocity fields.

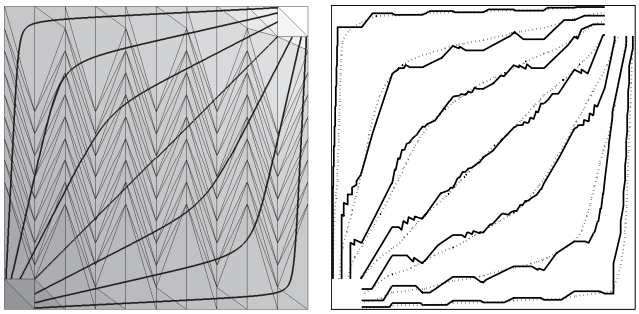

Fig. 12—Left: pressure solution on the triangular chevron grid and reference streamlines. Right: streamlines traced on the triangular chevron grid with the RT_0 (solid lines) and BDM_1 (dotted lines) velocity fields.

TABLE 1—RELATIVE TIME OF FLIGHT ERROR FOR EACH STREAMLINE TRACED ON THE CHEVRON GRIDS

	Quadrilaterals		Triangles	
SL #	RT_0 (%)	BDM_1 (%)	RT_0 (%)	BDM_1 (%)
1	26.50	7.92	12.99	6.91
2	5.05	5.04	2.70	2.62
3	4.07	1.37	1.92	1.42
4	11.23	1.61	12.09	3.44
5	3.66	1.33	2.70	0.35
6	4.84	1.21	2.50	0.95
7	55.56	5.57	26.95	6.47
Average	15.84	3.43	8.84	3.17

Clearly, for both the quadrilateral and the triangular grids, the streamlines obtained with the BDM_1-based flux reconstruction technique are more accurate, both in terms of actual location and time of flight. In addition, we recall that this increased accuracy of the BDM_1-based tracing is obtained with the same computational cost and memory requirements as the RT_0 streamlines.

To understand the importance of the time-of-flight accuracy, we focus our attention on the diagonal streamline (the fourth streamline from the top). In the simulation of an injection problem, the time-of-flight along this diagonal streamline would provide the breakthrough time of the injected fluid. We see that using the RT_0-based tracing, which is Pollock's method corrected for grid distortion and full tensor permeabilities, would lead to a 11% error in the estimated breakthrough time. The use of the BDM_1-based tracing reduces this error to under 2%.

Unstructured Grid. This last example represents a reservoir composed of two rock types, a base rock of relatively high permeability and a low-permeability rock forming three flow barriers. The permeability of the base rock presents a 10:1 anisotropy ratio and its principal directions are rotated by a 15° angle from the coordinate system:

$$k = R^t \begin{pmatrix} 10 & 0 \\ 0 & 1 \end{pmatrix} R \approx \begin{pmatrix} 9.40 & 2.25 \\ 2.25 & 1.60 \end{pmatrix}, \quad \ldots\ldots\ldots \quad (29)$$

with the rotation matrix R defined as in Eq. 28. The rock forming the flow barriers is isotropic and of permeability 10^{-3}.

The domain boundaries are impervious. An injector of unit pressure is placed at the bottom left of the domain and a producer of zero pressure is located in the top right corner. To describe accurately the geometry of the flow barriers and the well locations, two unstructured triangular grids are defined. The coarse, 599-element grid is shown on **Fig. 13** and the finer 4,841-element grid is presented in **Fig. 14.**

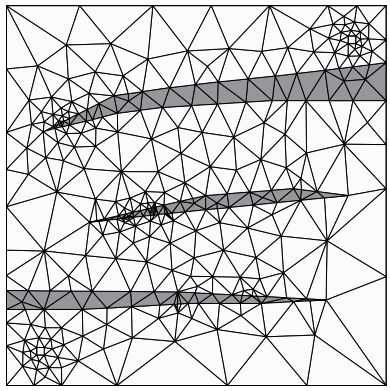

Fig. 13—Coarse unstructured grid and permeability field.

On the coarser grid, MPFA is used to solve the flow problem and streamlines are traced using the RT_0 and BDM_1 velocity field reconstruction. Ten streamlines are launched from the edges of the injecting well and traced all the way to the edges of the producing well. **Fig. 16** shows the launching points of the streamlines and presents their numbering. **Fig. 15** compares the streamlines obtained on the coarse grid with the RT_0- and BDM_1-based tracing methods.

On the fine grid, a BDM_1 mixed finite element method is used to solve for the pressure and velocity fields and to trace the streamlines presented in Fig. 14 that we use as reference.

Table 2 presents the relative errors in time-of-flight for the ten streamlines traced on the coarse grid with the RT_0 and the BDM_1 velocity fields. Once again, the results show how the BDM_1-based tracing algorithm provides superior streamlines than the RT_0-based method, both in terms of location and time-of-flight. It is interesting to notice that the fifth and sixth streamlines traced with the RT_0 velocity field present the largest time-of-flight errors. The corresponding BDM_1-based streamlines are more than twice as accurate. Because of their central location, these streamlines have the highest velocities and shortest time-of-flight so that they carry the most flow between the two wells. Therefore, in this example, the BDM_1 tracing is expected to have a large positive impact on the overall accuracy of the streamline method.

Conclusions

In this paper, we present a streamline tracing method for MPFA discretizations on general triangular or quadrilateral grids. The velocity field is reconstructed by interpolation of the MPFA subfluxes to recover a linear velocity profile across edges. This interpolation is based on the first order Brezzi-Douglas-Marini space (BDM_1). The streamline path is obtained analytically since the stream function for a BDM_1 velocity field is known (Juanes and Matringe In Press). The time-of-flight is however too complex to yield an analytical expression and is therefore integrated numerically.

Our numerical experiments show that in the presence of misaligned anisotropic permeability or grid distortion, the higher-order

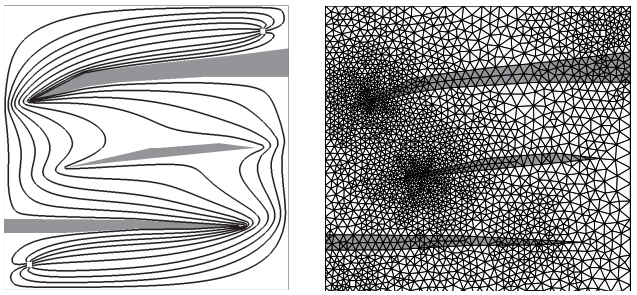

Fig. 14—Streamlines (left) traced on the reference unstructured grid (right).

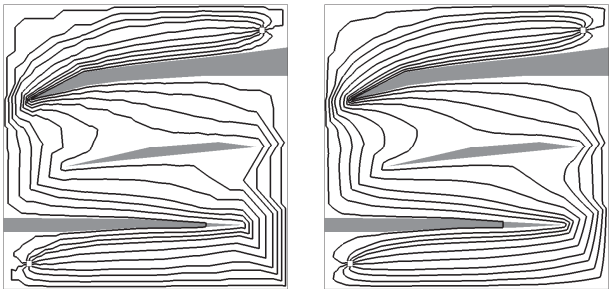

Fig. 15—Streamlines traced on the coarse unstructured grid with the RT_0-based (left) and BDM_1-based (right) tracing.

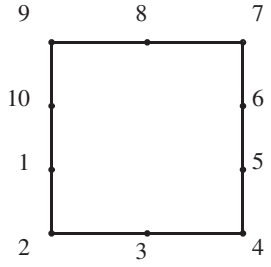

Fig. 16—Location of the streamline launching points on the edges of the gridcell containing the injection well.

TABLE 2—RELATIVE TIME OF FLIGHT ERROR FOR THE STREAMLINES TRACED ON THE UNSTRUCTURED GRID

SL #	RT_0 (%)	BDM_1 (%)
1	3.94	1.37
2	5.61	3.01
3	7.88	4.37
4	9.86	7.08
5	20.15	8.50
6	17.84	8.03
7	12.13	8.23
8	8.80	6.90
9	7.22	4.72
10	11.71	10.60
Average	10.51	6.28

velocity reconstruction based on BDM_1 recovers more accurate streamlines and time-of-flight than existing methods based on RT_0 velocity fields such as Pollock's method (Pollock 1988) or its extension to general quadrilaterals (Cordes and Kinzelbach 1992). It is important to note that no extra computational cost is associated to this gain in accuracy. The subfluxes used for the velocity reconstruction are already computed by the MPFA method. Therefore, our approach does not require a flux recovery procedure and tracing on a finer grid, as in the method by Prévost et al. (2002).

The proposed streamline tracing algorithm provides a rigorous extension of the streamline method to general triangular or quadrilateral grids populated with tensor permeabilities. Finally, we note that the velocity reconstruction technique presented here extends naturally to 3D grids (Matringe et al. 2007a; Matringe et al. 2009) and will be the subject of an upcoming publication.

Nomenclature

D	=	Jacobian matrix of the mapping
f	=	fractional flow function
F	=	flux out of a control volume
F_i	=	flux associated with the i^{th} edge of the grid
g	=	source term
J	=	determinant of the Jacobian matrix D
k	=	permeability tensor
$\hat{K}$	=	reference element
K_i	=	i^{th} control volume
$\mathcal{L}$, $\hat{\mathcal{L}}$	=	streamline in the real and reference space
n	=	outward pointing normal to a boundary
N	=	number of gridcells
N_a	=	shape function associated with the a^{th} node
p	=	pressure
$\mathcal{P}$	=	Piola transform
p_j	=	average pressure of the j^{th} gridblock
S	=	saturation
t	=	time in the real space
T_{ij}	=	transmissibility coefficient associated with the i^{th} edge and the j^{th} pressure node
u, $\hat{u}$	=	Darcy velocity in the physical and reference space
u_x, u_y	=	x- and y- components of u
x, $\hat{x}$	=	coordinates in the physical and reference space
Γ	=	edge or boundary
λ	=	total fluid mobility
τ	=	time-of-flight
φ	=	isoparametric mapping
Ψ	=	stream function
Ω	=	simulation domain

Acknowledgments

The authors gratefully acknowledge financial support from the members of the affiliate program of the Stanford University Petroleum Research Institute for Reservoir Simulation.

References

Aavatsmark, I. 2002. An introduction to multipoint flux approximations for quadrilateral grids. *Computational Geosciences* **6** (3–4): 405–432. DOI:10.1023/A:1021291114475.

Aavatsmark, I., Barkve, T., Bøe, Ø., and Mannseth, T. 1996. Discretization on non-orthogonal, quadrilateral grids for inhomogeneous, anisotropic media. *Journal of Computational Physics* **127** (1): 2–14. DOI:10.1006/jcph.1996.0154.

Aavatsmark, I., Barkve, T., Bøe, Ø., and Mannseth, T. 1998b. Discretization on unstructured grids for inhomogeneous, anisotropic media. Part I: Derivation of the methods. *SIAM Journal on Scientific Computing* **19** (5): 1700–1716. DOI:10.1137/S1064827595293582.

Aavatsmark, I., Barkve, T., Bøe, Ø., and Mannseth, T. 1998c. Discretization on unstructured grids for inhomogeneous,

anisotropic media. Part II: Discussion and numerical results. *SIAM Journal on Scientific Computing* **19** (5): 1717–1736. DOI:10.1137/S1064827595293594.

Aavatsmark, I., Barkve, T., and Mannseth, T. 1998a. Control-Volume Discretization Methods for 3D Quadrilateral Grids in Inhomogeneous, Anisotropic Reservoirs. *SPEJ* **3** (2): 146–154. SPE-38000-PA. DOI:10.2118/38000-PA.

Aziz, K. and Settari, A. 1979. *Petroleum Reservoir Simulation*, London: Elsevier.

Babuška, I. 1973. The finite element method with Lagrangian multipliers. *Numerische Mathematik* **20** (3): 179–192. DOI:10.1007/BF01436561.

Batycky, R.P., Blunt, M.J., and Thiele, M.R. 1997. A 3D Field-Scale Streamline-Based Reservoir Simulator. *SPERE* **12** (4): 246–254. SPE-36726-PA. DOI:10.2118/36726-PA.

Bratvedt, F., Bratvedt, K., Buchholz, C.F., Gimse, T., Holden, H., Holden, L., and Risebro, N. H. 1993. Frontline and Frontsim: Two full scale, two-phase, black oil reservoir simulators based on front tracking. *Surveys on Mathematics for Industry* **3** (3): 185–215.

Brenner, S.C. and Scott, L.R. 1994. *The Mathematical Theory of Finite Element Methods*, New York: Texts in Applied Mathematics Series, Springer-Verlag.

Brezzi, F. 1974. On the existence, uniqueness and approximation of saddle point problems arising from Lagrange multipliers. *RAIRO Anal. Numér.* **8**:129–151.

Brezzi, F., Douglas, Jr., J., and Marini, L.D. 1985. Two families of mixed finite elements for second order elliptic problems. *Numerische Mathematik* **47** (2): 217–235. DOI:10.1007/BF01389710.

Brezzi, F. and Fortin, M. 1991. *Mixed and Hybrid Finite Element Methods*, Vol. 15. Berlin: Springer Series in Computational Mathematics Series, Springer-Verlag.

Cordes, C. and Kinzelbach, W. 1992. Continuous groundwater velocity fields and path lines in linear, bilinear, and trilinear finite elements. *Water Resources Research* **28** (11): 2903–2911. DOI:10.1029/92WR01686.

Datta-Gupta, A. and King, M.J. 1995. A semianalytic approach to tracer flow modeling in heterogeneous permeable media. *Advances in Water Resources* **18** (1): 9–24. DOI:10.1016/0309-1708(94)00021-V.

Dormand, J.R. and Prince, P.J. 1980. A family of embedded Runge-Kutta formulae. *J. Comput. Appl. Math.* **6** (1): 19–26. DOI:10.1016/0771-050X(80)90013-3.

Edwards, M.G. 2002. Unstructured, control-volume distributed, full-tensor finite-volume schemes with flow based grids. *Computational Geosciences* **6** (3–4): 433–452. DOI:10.1023/A:1021243231313.

Edwards, M.G. and Rogers, C.F. 1998. Finite-volume discretization with imposed flux continuity for the general tensor pressure equation. *Computational Geosciences* **2** (4): 259–290. DOI:10.1023/A:1011510505406.

Hægland, H., Dahle, H.K., Eigestad, G.T., Lie, K.-A., and Aavatsmark, I. 2007. Improved streamlines and time-of-flight for streamline simulation on irregular grids. *Advances in Water Resources* **30** (4): 1027–1045. DOI:10.1016/j.advwatres.2006.09.002.

Jimenez, E., Sabir, K., Datta-Gupta, A., and King, M.J. 2007. Spatial error and convergence in streamline simulation. *SPEREE* **10** (3): 221–232. SPE-92873-PA. DOI:10.2118/92873-PA.

Juanes, R. and Matringe, S.F. In Press. Unified formulation for high-order streamline tracing on two-dimensional unstructured grids. *Journal of Scientific Computing*, (accepted 2006). DOI:10.1007/s10915-008-9228-2.

King, M.J. and Datta-Gupta, A. 1998. Streamline simulation: A current perspective. *In Situ* **22** (1): 91–140.

Lee, S.H., Jenny, P., and Tchelepi, H.A. 2002a. A finite-volume method with hexahedral multiblock grids for modeling flow in porous media. *Computational Geosciences* **6** (3–4): 353–379. DOI:10.1023/A:1021287013566.

Lee, S.H., Tchelepi, H., Jenny, P., and DeChant, L.F. 2002b. Implementation of a flux-continuous finite-difference method for stratigraphic, hexahedron grids. *SPEJ* **7** (3): 267–277. DOI:10.2118/80117-PA

Marsden, J.E. and Hughes, T.J.R. 1994. *Mathematical Foundations of Elasticity*, Mineola, New York: Dover Publications, Inc.

Matringe, S.F., Juanes, R., and Tchelepi, H.A. 2006. Robust streamline tracing for the simulation of porous media flow on general triangular and quadrilateral grids. *J. Comput. Phys.* **219** (2): 992–1012. DOI:10.1016/j.jcp.2006.07.004.

Matringe, S.F., Juanes, R., and Tchelepi, H.A. 2007a. Mixed Finite-Element and Related Control Volume Discretizations for Reservoir Simulation on Three-Dimensional Unstructured Grids. Paper SPE-106117-MS presented at the SPE Reservoir Simulation Symposium, Houston, 26–28 February. DOI:10.2118/106117-MS.

Matringe, S.F., Juanes, R., and Tchelepi, H.A. 2007b. Streamline Tracing on General Triangular or Quadrilateral Grids. *SPEJ* **12** (2): 217–233. SPE-96411-PA. DOI:10.2118/96411-PA.

Matringe, S.F., Juanes, R., and Tchelepi, H.A. 2009. Convergence of MPFA on Hexahedra. Paper SPE-119203-MS presented at the SPE Reservoir Simulation Symposium, Houston, 2–4 February.

Mosé, R., Siegel, P., Ackerer, P., and Chavent, G. 1994. Application of the mixed hybrid finite element approximation in a groundwater flow model: Luxury or necessity?. *Water Resources Research* **30** (11): 3001–3012. DOI:10.1029/94WR01786.

Pollock, D.W. 1988. Semianalytical computation of path lines for finite-difference models. *Ground Water* **26** (6): 743–750. DOI:10.1111/j.1745-6584.1988.tb00425.x.

Prévost, M., Edwards, M.G., and Blunt, M.J. 2002. Streamline Tracing on Curvilinear Structured and Unstructured Grids. *SPEJ* **7** (2): 139–148. SPE-78663-PA. DOI:10.2118/78663-PA.

Raviart, P.A. and Thomas, J.M. 1977. A mixed finite element method for second order elliptic problems. In *Mathematical Aspects of the Finite Element Methods: Proceedings of the Conference Held in Rome, December 10–12, 1975*, ed. I. Galligani and E. Magenes, Vol. 606, 292–315. New York: Lecture Notes in Mathematics, Springer-Verlag.

Verma, S. and Aziz, K. 1997. A control volume scheme for flexible grids in reservoir simulation. Paper 37999 presented at the SPE Reservoir Simulation Symposium, Dallas, 8–1 June. DOI:10.2118/37999-MS, June 8–11.

Sébastien F. Matringe is a reservoir engineer at Chevron Energy Technology Co. His main research interest is reservoir simulation on unstructured grids, including streamline methods, mixed finite element methods, and multipoint flux approximation methods. He holds a *diplôme d'ingénieur* in mechanical engineering from the École Nationale Supérieure d'Électronique, d'Électrotechnique, d'Informatique, d'Hydraulique, et des Télécommunications, in Toulouse, France, and MS and PhD degrees in petroleum engineering from Stanford University. **Ruben Juanes** is the ARCO Assistant Professor in Energy Studies, in the department of civil and environmental engineering at the Massachusetts Institute of Technology. Before joining the MIT faculty in 2006, he was an acting assistant professor in petroleum engineering at Stanford University (2003-2005), and an assistant professor in petroleum and geosystems engineering at the University of Texas at Austin (2006). His current research interests

are reservoir simulation (including mixed finite element, streamline, and variational multiscale methods), geological CO2 sequestration, and methane hydrates in ocean sediments. He holds MS and PhD degrees in civil and environmental engineering from the University of California at Berkeley. **Hamdi A. Tchelepi** is associate professor in the Dept. of Energy Resources Engineering at Stanford University. Prior to joining Stanford in 2003, he was a research scientist with Chevron Energy Technology Co. He is interested in building computational frameworks for reservoir simulation and subsurface carbon sequestration. Specific research interests include modeling unstable flow processes, stochastic numerical methods for uncertainty quantification, and multiscale formulations for multiphase flow and transport. He holds a PhD degree in petroleum engineering from Stanford University.